Terahertz wire grid polarizer fabricated by imprinting porous silicon

Imakita, Kenji ; Kamada, Takeshi ; Fujii, Minoru ; Aoki, Kanna ; Mizuhata, Minoru ; Hayashi, Shinji

(Citation)
Optics Letters,38(23):5067-5070

(Issue Date)
2013

(Resource Type)
journal article

(Version)
Version of Record

(URL)
https://hdl.handle.net/20.500.14094/90002570

Terahertz wire grid polarizer fabricated by imprinting porous silicon

Kenji Imakita,* Takeshi Kamada, Minoru Fujii, Kanna Aoki, Minoru Mizuhata, and Shinji Hayashi

Department of Electrical and Electronic Engineering, Graduate School of Engineering, Kobe University, Rokkodai, Nada, Kobe, 657-8501, Japan

**Corresponding author: imakita@eedept.kobe-u.ac.jp*

Received September 9, 2013; revised October 28, 2013; accepted October 28, 2013; posted October 28, 2013 (Doc. ID 197420); published November 25, 2013

A terahertz (THz) wire-grid polarizer is fabricated by imprinting porous Si followed by oblique evaporation of Ag. We demonstrate that it works in a wide frequency region covering from 5 to 18 THz with the extinction ratio of 10 dB. The frequency region is much wider than that of THz wire-grid polarizers fabricated by conventional imprint lithography using organic materials. The result suggests that imprinting of porous Si is a promising fabrication technique to realize low-cost wire-grid polarizers working in the THz region.

OCIS codes: (050.1970) Diffractive optics; (230.5440) Polarization-selective devices.
http://dx.doi.org/10.1364/OL.38.005067

With the recent development of terahertz (THz) technologies, there has been a growing demand for the development of low-cost and high-performance THz optical elements [1–4]. An example is a wire-grid polarizer (WGP), which is an essential optical element for THz imaging and spectroscopy [5–7]. Commercially available WGPs consist of the array of well-aligned and uniformly spaced free-standing metal wires with a periodicity of several μm fabricated by mechanical processes [8]. However, precise alignment of fine meal wires by a mechanical process is still a challenging and high-cost task.

An alternative fabrication process is the formation of Al wires on a Si substrate by photolithography. Because of the precise alignment of Al wires, high extinction ratio (30 dB) is achieved [9]. Another more cost-effective alternative is the process that uses imprinting. Takano *et al.* [10] realized a WGP with Al wires on a triacetylcellulose film by ultraviolet nanoimprint lithography followed by oblique evaporation of Al. The process is much simpler than mechanical or photolithographic process and thus higher throughput can be expected. However, organic materials, which are commonly used as imprint materials, are generally not transparent in the THz region due to the absorption arising from vibration modes of carbon–hydrogen bonds. This limits the working frequency region of WGPs fabricated by imprint lithography. In fact, in [10], the WGP works in the frequency region only below 2 THz.

In order to realize a WGP with a wider frequency region by imprint lithography, we prepared porous Si as an imprint material for the first time. Porous Si is known to be highly transparent in the THz region because crystalline Si is infrared inactive. Some kinds of THz devices utilizing the high transparency of porous Si have been reported [11,12]. In addition, as reported by Ryckman *et al.* [13], porous Si can be imprinted with high resolution at room temperature in air due to the compressibility of the porous network. In this work, we fabricate WGPs by imprinting porous Si and demonstrate that it works as a polarizer in a wide frequency region covering from 5 to 18 THz, with the extinction ratio of about 10 dB for the whole frequency region. Our results suggest that the imprinting of porous Si is a promising fabrication technique for the production of low-cost WGPs working in the THz region.

The fabrication process of the WGP consists of three steps as shown in Fig. 1. First, porous Si was prepared by electrochemical etching of Si wafers. It was then imprinted by a quartz mold to print a grating structure. Finally Ag was obliquely evaporated onto the porous Si to form Ag wires on the grating structure.

For the preparation of porous Si, (100) oriented *p*-type Si wafers with the resistivity of 11–15 Ωcm were used as an initial wafer. The wafers are much more resistive than those used for porous Si for nano-imprinting (0.01–0.02 Ωcm) [11]. The highly resistive wafers are transparent in the THz region due to the low carrier concentration and are favorable for the application to THz WGPs. The electrochemical etching was performed in a solution of 7:3 by volume mixture of hydrofluoric acid (46 wt. %) and ethanol with the anodic current density of 80 mA/cm^2. The thickness of porous Si is set to about 40 μm, which is much thicker than the imprint depth (1 μm), to avoid damage to a quartz mold. The samples were characterized using a field emission scanning electron microscope (FESEM) (JEOL-JSM6335F) operated at 13 kV and a transmission electron microscope (TEM) (JEOL-JEM-2010) operated at 200 kV. Figure 2(a) shows a TEM image of the porous Si. It consists of Si nanocolumns smaller than 10 nm. The size of pores between Si nanocolumns is smaller than 5 nm. This is an order of magnitude smaller than that reported in the previous work on the imprinting of porous Si [13]. The small structures are due to the high resistivity of the initial Si wafers [14], and similar TEM images were reported in [15]. Figure 2(b) shows the reflectance spectrum. An interference fringe can be seen, which confirms high uniformity

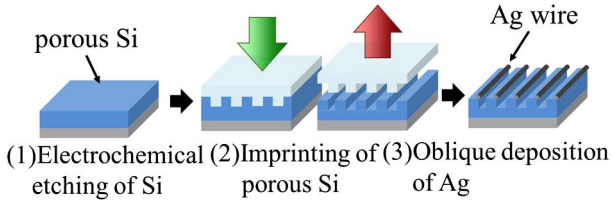

Fig. 1. Schematic of fabrication processes of a WGP.

0146-9592/13/235067-04$15.00/0

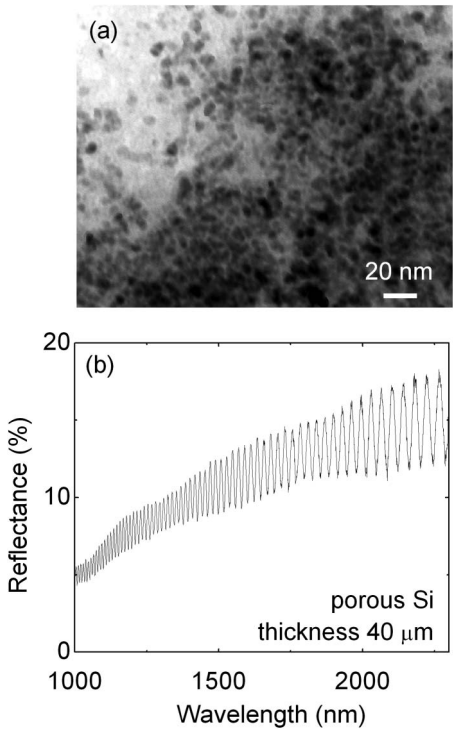

Fig. 2. (a) TEM image of a porous Si layer. (b) Reflectance spectrum of a porous Si layer on a Si substrate. Thickness of the porous Si layer is about 40 μm.

of the porous Si film. The effective refractive index of the porous Si film (n_{eff}) was calculated from the thickness (b) and peak wavelengths of the interference fringe by using the relation

$$2n_{\text{eff}}d = 1/(1/\lambda_n - 1/\lambda_{n+1}),$$

where λ_n is the wavelength of the nth peak [16]. The calculation reveals that n_{eff} is about 1.45 in the near infrared region. From the relation between n_{eff} and the porosity [17], the porosity of the present sample is estimated to be 60–70%.

Imprinting of porous Si was conducted at room temperature in air by using a commercial quartz mold (NTT advanced technology, NIM-1000UL). The periodicity and height of the grating are 2 and 1 μm, respectively. The patterned area is 36 mm^2 (6×6 mm), and the mold thickness is 0.6 mm. The mold was treated in a release agent (HARVES, DS-5210TH) to make the surface hydrophobic. During the imprinting, 20 MPa was applied for 1 min. This pressure is much lower than that reported in the previous work on the imprinting of porous Si (100–400 MPa) [13]. The different morphology and/or different thickness of porous Si films may allow us to reduce the imprinting pressure.

Figure 3(a) shows a SEM image of the sample after imprinting. We can see that a grating structure of the mold is well transferred to the surface of the porous Si. Figure 3(b) is the enlarged view. The imprinted surface is very smooth, which is favorable for the application to THz WGPs. In the scale of Fig. 3(b), porous structures cannot be observed due to the very small size of nanocolumns and pores. This is different from the

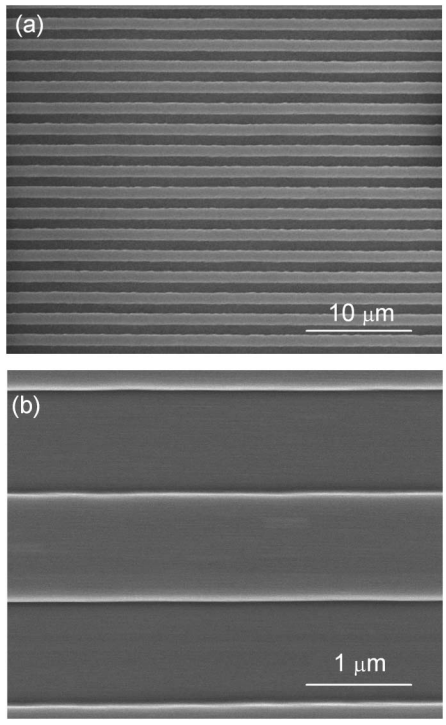

Fig. 3. (a) Plan-view FESEM images of the imprinted porous Si. (b) Enlarged view.

work by Ryckman *et al.* on the imprinting of mesoporous Si, which consists of the structures of several tens of nm [13].

Ag wires were formed on the imprinted porous Si by oblique evaporation of Ag. The porous Si sample was tilted by 85° from the evaporation direction. The source-to-sample distance was 10 cm. Figure 4(a) shows

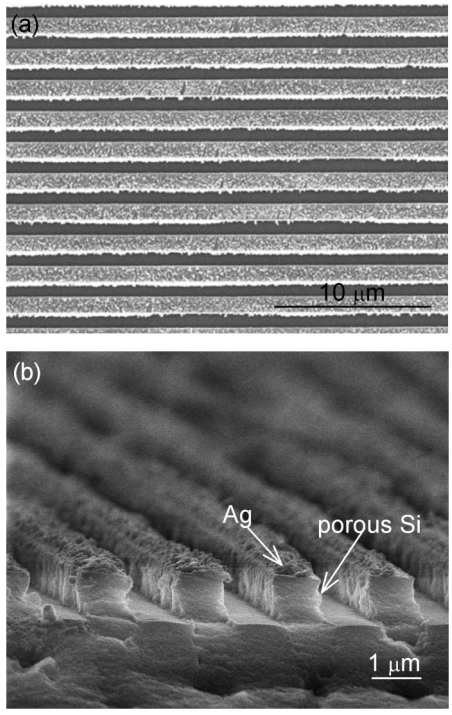

Fig. 4. (a) Plan-view and (b) cross-sectional FESEM images of the imprinted porous Si after the oblique evaporation of Ag.

a plan-view FESEM image of the sample after the oblique evaporation of Ag. By comparing Figs. 3(a) and 4(a), we can see that the top surface of the grating becomes rough by the oblique evaporation, while the bottom surface remains relatively smooth. The rough region corresponds to the deposited Ag film. The area ratio of the Ag-deposited region is about 0.55, which is optimum to simultaneously achieve the high extinction ratio and the high transmittance [18]. Figure 4(b) shows a cross-sectional SEM image of the same sample. The height of the grating is 1 μm, suggesting that the grating pattern is fully transferred into the porous Si. We can see that an array of Ag wires is formed on the top surface of the grating structure. The thickness of the Ag wires is 0.1–0.3 μm. Note that similar structure can be produced by Al and Au, whose absorption losses are negligible and similar to that of Ag in the THz region.

Figure 5 shows the transmittance spectra of a Si wafer (p-type 11–15 Ωcm), that on which porous Si film is formed (porous Si/Si) and that on which porous Si and a Ag wire grid are formed (Ag WG/porous Si/Si), respectively. These spectra are measured by a Fourier transform infrared spectrometer (FT-IR; Perkin Elmer, Spectrum GX), which covers the frequency range of 1–300 THz. The transmittance of the Si substrate is about 50%, due to the high reflectance (~50%) caused by the high refractive index [19]. The formation of porous Si (porous Si/Si) does not decrease the transmittance around 5 THz, while it does at higher frequencies. The decrease is due to the absorption of vibration modes of silicon–oxygen bonds on the surface of porous Si [20]. The two small dips around 7 and 10 THz are due to interference of light in the porous Si film. The transmittance of the Ag WG/porous Si/Si is about the half of that of the porous Si/Si. This implies that the Ag WG/porous Si/Si structure works as a polarizer with a small absorption loss, because 50% of unpolarized light can path through an ideal polarizer, according to the Malus' law [21].

The inset of Fig. 6(a) shows the optical setup for the evaluation of the performance of the WGP. The setup is installed in the FT-IR. We divided a sample into two (sample A and B). Sample A is used to produce linearly polarized light from the unpolarized light source.

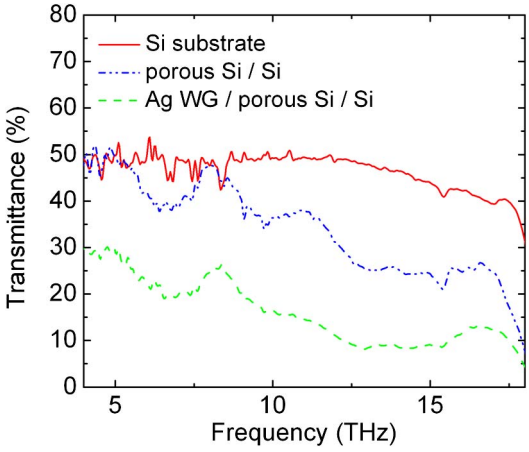

Fig. 5. Transmittance spectra of the Si substrate, the porous Si/Si, and the Ag WG/porous Si/Si, for unpolarized light.

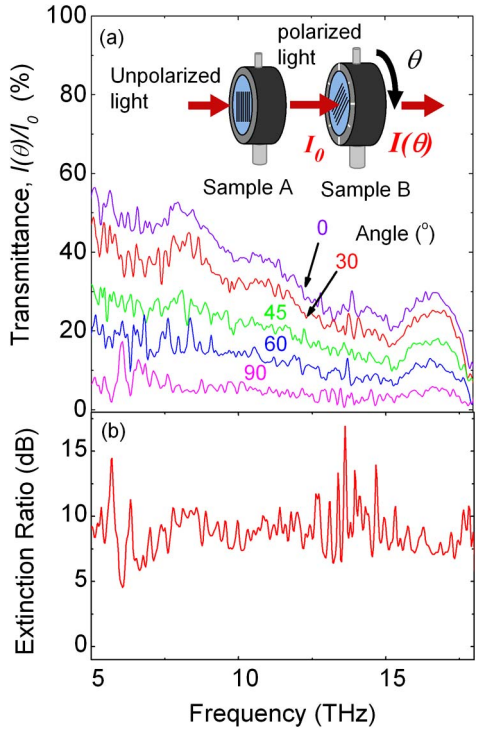

Fig. 6. (a) Transmittance spectra of the stack of the two WGPs as a function of the mutual angle between the two polarizing axes. The spectra are normalized with respect to that of a single polarizer for unpolarized light. (b) Extinction ratio of the WGP estimated from the transmittance spectra.

Sample B is rotated about the optical axis and the transmittance ($I(\theta)/I_0$) is measured as a function of the angle (θ), where I_0 is the transmittance when sample B is removed. $\theta = 0°$ corresponds to the mutual angle of 0°. Figure 6(a) shows the transmittance as a function of θ. When $\theta = 0°$, the transmittance reaches 50% in the low frequency region (<8 THz). This value is similar to that of the Si substrate, implying that the transmittance loss is mainly caused by the reflectance of Si substrate. With increasing θ, the transmittance decreases, and takes the minimum when $\theta = 90°$. In Fig. 6(b), the extinction ratio defined by $-10\log(T_\perp/T_\parallel)$, where $T_\parallel$ and $T_\perp$ are $I(0°)/I_0$ and $I(90°)/I_0$, respectively, is plotted. It is about 10 dB for the whole frequency region.

In order to discuss our results more quantitatively, we calculated the transmittance by using a simulation package (RSoft, DiffractMOD) employing a rigorous coupled wave analysis. In Fig. 7(a), the calculation model is shown. The thickness of Si substrate, porous Si film, the imprinted layer, and the deposited Ag film are 700, 40, 1, and 0.15 μm, respectively. In the near to far infrared region (1.5–100 μm or 3–200 THz), the dispersion of the refractive index of Si is very small and the imaginary part is almost zero. Therefore, the effective refractive index of porous Si is set to the same value as that estimated in the near infrared region (1.45) with no imaginary part. The refractive index of Si is 3.48 [22]. The curve in figure 7(b) shows the calculated transmittance at 10 THz as a function of θ. We can see that the calculated transmittance (the solid line) almost agrees with the experimentally obtained values (the open square). For

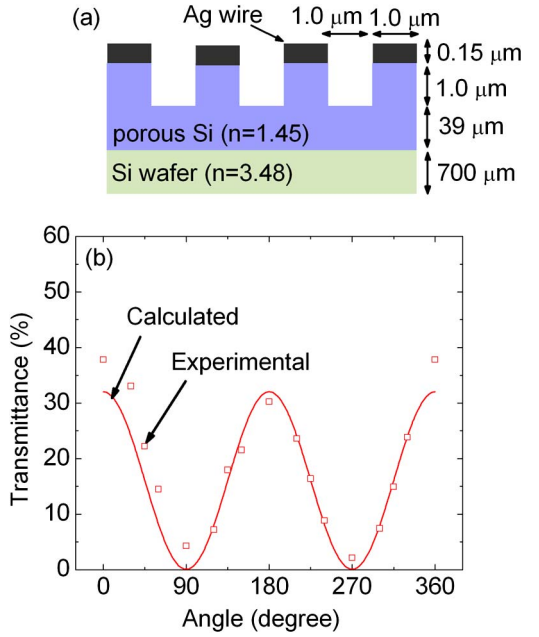

Fig. 7. (a) Calculation model for the WGP fabricated in this work. (b) Transmittance of the stack of the two WGPs at 10 THz as a function of the mutual angle between the two polarizing axes. The solid line and the open square are calculated and experimental results, respectively.

example, when θ equals to 0°, 180°, and 360°, both the measured and calculated transmittances take maxima. Furthermore, the gap between them is less than 5%. This confirms that the transmittance loss is due to neither absorption nor scattering by the WGP structure. It is due to the reflectance of the Si substrate. Therefore, the transmittance can be improved by removing the Si substrate and using free-standing porous Si [23] or by the formation of anti-reflection layers. On the other hand, the observed extinction ratio is much smaller than the calculated value. By using the calculated values of $T_{\parallel}$ (32.0%) and $T_{\perp}$ (0.093%), the extinction ratio is estimated to be about 25 dB at 10 THz. This is 16 dB larger than the experimental result (9 dB). A possible origin of the difference is light scattering by the roughness of Ag wires. This may be improved by optimization of Ag deposition processes.

In conclusion, we fabricated a WGP by imprinting of porous Si and following oblique evaporation of Ag. We demonstrated that it works as a polarizer in a wide frequency region covering from 5 to 18 THz. The working range is much wider than that of WGPs fabricated by conventional imprint lithography using organic materials. Our result suggests that the room-temperature imprinting of porous Si is a promising approach to realize low-cost WGPs working in the THz region.

This work is partly supported by research grants from "The Kyoto Technoscience Center" and "The Center for Collaborative Research and Technology Development (CREATE) of Kobe University".

References

1. M. Sypek, M. Makowski, E. Hérault, A. Siemion, A. Siemion, J. Suszek, F. Garet, and J.-L. Coutaz, Opt. Lett. **37**, 2214 (2012).
2. S. C. Saha, Y. Ma, J. P. Grant, A. Khalid, and D. R. S. Cumming, Opt. Express **18**, 12168 (2010).
3. E. D. Walsby, Opt. Lett. **32**, 1141 (2007).
4. J.-B. Masson and G. Gallot, Opt. Lett. **31**, 265 (2006).
5. N. C. J. van der Valk, W. A. M. van der Marel, and P. C. M. Planken, Opt. Lett. **30**, 2802 (2005).
6. I. Yamada, K. Kintaka, J. Nishi, S. Akioka, Y. Yamagishi, and M. Saito, Opt. Lett. **33**, 258 (2008).
7. D. Kim, Appl. Opt. **44**, 1366, 2005.
8. C. L. Mok, W. G. Chambers, T. J. Parker, and A. E. Costley, Infrared Phys. **19**, 437 (1979).
9. I. Yamada, K. Takano, M. Hangyo, M. Saito, and W. Watanabe, Opt. Lett. **34**, 274 (2009).
10. K. Takano, H. Yokoyama, A. Ichii, I. Morimoto, and M. Hangyo, Opt. Lett. **36**, 2665 (2011).
11. S. Z. A. Lo and T. E. Murphy, Opt. Lett. **34**, 2921 (2009).
12. S. Z. A. Lo and T. M. Murphy, Appl. Phys. Lett. **96**, 201104 (2010).
13. J. D. Ryckman, M. Liscidini, J. E. Sipe, and S. M. Weiss, Nano Lett. **11**, 1857 (2010).
14. A. G. Cullis, L. T. Canham, and P. D. J. Calcott, J. Appl. Phys. **82**, 909 (1997).
15. A. G. Cullis and L. T. Canham, Nature **353**, 335 (1991).
16. C. Pickering, M. I. J. Beale, D. J. Robbins, P. J. Pearson, and R. Greef, Thin Solid Films **125**, 157 (1985).
17. M. Khardani, M. Bouaïcha, and B. Bessaïs, Phys. Stat. Sol. **4**, 1986 (2007).
18. P. Yeh, Opt. Commun. **26**, 289 (1978).
19. I. Yamada, K. Fukumi, J. Nishii, and M. Saito, Opt. Lett. **35**, 3111 (2010).
20. W. Theiss, Sur. Sci. Rep. **29**, 91 (1997).
21. D. S. Kliger, J. W. Lewis, and G. E. Randall, *Polarized Light Optics and Spectroscopy* (Academic, 1990).
22. H. W. Icenogle, B. C. Platt, and W. L. Wolfe, Appl. Opt. **15**, 2348 (1976).
23. Y. Kanemitsu, H. Uto, and Y. Masumoto, Phys. Rev. B **48**, 2827 (1993).